Reactive scattering dynamics of rotational wavepackets: A case study using the model H+H2 and F+H2 reactions with aligned and anti-aligned H2

C. J. Eyles and M. Leibscher

Citation: The Journal of Chemical Physics **139**, 104315 (2013); doi: 10.1063/1.4820881
View online: http://dx.doi.org/10.1063/1.4820881
View Table of Contents: http://scitation.aip.org/content/aip/journal/jcp/139/10?ver=pdfcov
Published by the AIP Publishing

Reactive scattering dynamics of rotational wavepackets: A case study using the model H+H_2 and F+H_2 reactions with aligned and anti-aligned H_2

C. J. Eyles[1] and M. Leibscher[2]
[1]*Institut für Chemie und Biochemie, Freie Universität Berlin, 14195 Berlin, Germany*
[2]*Institut für Theoretische Physik, Leibniz Universität Hannover, 30167 Hannover, Germany*

(Received 12 June 2013; accepted 27 August 2013; published online 13 September 2013; corrected 18 September 2013)

We propose a method to steer the outcome of reactive atom-diatom scattering, using rotational wavepackets excited by strong non-resonant laser pulses. Full close-coupled quantum mechanical scattering calculations of the D+H_2 and F+H_2 reactions are presented, where the H_2 molecule exists as a coherent superposition of rotational states. The nuclear spin selective control over the molecular bond axis alignment afforded by the creation of rotational wavepackets is applied to reactive scattering systems, enabling a nuclear spin selective influence to be exerted over the reactive dynamics. The extension of the conventional eigenstate-to-eigenstate scattering problem to the case in which the initial state is composed of a coherent superposition of rotational states is detailed, and a selection of example calculations are discussed, along with their mechanistic implications. The feasibility of the corresponding experiments is considered, and a suitable simple two pulse laser scheme is shown to strongly differentiate the reactivities of *o*-H_2 and *p*-H_2. © *2013 AIP Publishing LLC*. [http://dx.doi.org/10.1063/1.4820881]

I. INTRODUCTION

The collisions of molecules and atoms constitute one of the simplest and most ubiquitous of chemical events. Their collective outcomes determine and define all manner of physical and chemical macroscopic phenomena, while their detailed understanding yields invaluable insight into the fundamental nature of the underlying physics. As such the experimental and theoretical study of inelastic and reactive collisions is a field that has seen extensive and sustained effort throughout the years.[1] The collisions of single atoms with diatomic molecules have received particular attention, since exact quantum mechanical calculations can be carried out for such systems, and it is also frequently possible to obtain fully quantum state-to-state resolved experimental data. The inherent simplicity of the problem also frequently enables a transparent mechanistic interpretation of the observed collision dynamics, allowing us to develop our chemical intuition.[2]

The relative configuration in which the particles encounter each other is instrumental in determining the unfolding of the collision event. Much mechanistic insight can be gained from a thorough investigation of this dependency, and it is even possible to dictate the outcome of a collision experiment by careful control of the colliding particles.[3,4] Conventionally, such control is achieved by using molecular beams to control the relative linear momenta of the colliding particles, and electromagnetic fields to influence the polarisation of either the molecular bond axis, **r**, or the molecular rotational angular momentum, **j**. More recently, sophisticated pulsed laser techniques have been developed which allow the polarisation of **r** or **j** via the creation of a rotational wavepacket, in which many different rotational levels coherently interfere with one another.[5–8] Tailored trains of laser pulses enable a high degree of control to be exerted over the spatial distribution of the molecular bond axis. The resulting polarisation exhibits a rich time-dependent structure as the various rotational levels come into and out of phase with one another, in addition to its time averaged value. Such methods offer a versatile alternative to conventional electromagnetic alignment methods. They are also somewhat more universal, since they enable, for example, the alignment of non-polar homonuclear diatomic molecules, and are compatible with the use of charged particles where electrostatic fields are not.[9]

An intriguing aspect of rotational wavepackets of symmetric molecules is that their time-evolution depends on the parity of the constituent rotational states. Consequently, nuclear spin modifications of the same chemical species show characteristic differences in their rotational dynamics, in particular in their time-dependent alignment.[10–12] Selective manipulation of nuclear spin modifications is thus a possible application of laser induced molecular alignment. Recently, it has been demonstrated that scattering of molecules at a surface[13] or in an inhomogeneous electric field[14,15] can be influenced by pre-exciting rotational wavepackets. Spinning molecules are scattered at different angles than rotationally cold molecules. It is suggested that the combination of nuclear spin selective control of rotational dynamics with surface scattering might lead to a spatial separation of nuclear spin modifications or other close chemical species, for example, molecular isotopes.[7]

In a similar spirit we consider atom-diatom collisions in the gas phase, and investigate how excitation of rotational wavepackets will influence the reactive encounter. It is known that nuclear spin can influence chemical reactions, and detailed nuclear spin selection rules have been derived.[16–20] Here, we excite different rotational wavepackets of the para and ortho nuclear spin modifications of H_2 prior to the

scattering event in order to control the reactive scattering in a nuclear spin selective manner. A theoretical treatment of the (fully quantum) scattering dynamics of a generalised rotational wavepacket is presented, and sample integral and differential cross-sections are presented for the reactive collisions of the model D+H_2 and F+H_2 systems.

The remainder of this paper is organised as follows: Sec. II A presents a basic summary of quantum scattering theory, along with the methodology typically used for calculating various quantities of interest. This treatment is extended from the conventional eigenstate-to-eigenstate situation to the case of a coherent superposition of initial rotational states, and expressions describing the scattering dynamics of such a rotational wavepacket are derived. In Sec. II B, we consider the creation of various rotational wavepackets exhibiting particular characteristics, using short non-resonant laser pulses. A brief overview of the scattering calculations conducted in this work is provided in Sec. II C. The results of our pilot studies on the scattering dynamics of three distinct classes of initial states in the D+H_2 and F+H_2 systems are then presented in Secs. III A and III B, where we consider initial eigenstates, fully coherent time resolved rotational wavepackets, and incoherent time averaged wavepackets. Within these sections, the mechanistic implications of the data are discussed, and the viability of the corresponding experimental studies is considered. Finally, Sec. IV presents our conclusions, and suggests some further areas of investigation which may yield interesting results in the future.

II. THEORY

In this section, the method by which the quantum mechanical scattering calculations performed in this work were carried out will be summarised, and expressions will be given relating the resulting $\hat{S}$-matrix elements to experimentally observable quantities of interest. The conventional expressions for the integral and differential cross-sections will be extended to describe the scattering dynamics of a coherent superposition of initial eigenstates, including rotational wavepackets. The creation of a rotational wavepacket using short pulses of non-resonant laser light will be outlined, allowing the definition of the pre-cursor in our collision studies. Finally, pertinent details relating to the calculations performed in this work are provided.

A. Calculation of quantum mechanical observables from the $\hat{S}$-matrix

The solution of the close-coupled equations describing the quantum mechanical scattering of a diatomic molecule with a structureless particle is a solved problem, and is now a relatively routine process.[21–24] Solution of these equations yields a set of $\hat{S}$-matrix elements specifying the individual channel-to-channel probability amplitudes. In reactive systems, such calculations are complicated by the different possible molecular arrangements in the entrance and exit channels; the "abc" quantum scattering code[24] employed in this work solves this ambiguity by simultaneously considering all three chemical arrangements using hyper-spherical co-ordinates, in which the problem becomes isomorphic to the simpler case of non-reactive inelastic scattering. The $\hat{S}$-matrix elements are calculated in the body fixed helicity frame, where the helicity quantum number specifies the projection of **j** onto the relative linear momentum of the atom-diatom pair.

One of the most elementary observables associated with a scattering event is the integral collision cross-section, which is related to the probability with which a collision effects a particular transition. The state-to-state resolved collision cross-sections can be written in terms of the helicity frame $\hat{T}$-matrix elements as

$$\sigma_{j'k'jk} = \frac{\pi}{k_{\text{vec}}^2} \sum_J (2J+1) \left| \langle j'k'|T^J|jk\rangle \right|^2. \qquad (1)$$

Here jk and $j'k'$ denote the rotational and helicity projection quantum numbers of the initial and final states, J is the total angular momentum quantum number, and k_{vec} is the wave-vector associated with the collision. The transition matrix element $\langle j'k'|T^J|jk\rangle$ gives the probability amplitude for the transition from the initial state $|jk\rangle$ to the final state $|j'k'\rangle$ for the Jth partial wave. The transition matrix ($\hat{T}$-matrix) itself is related to the scattering matrix via the expression $\hat{T} = \hat{1} - \hat{S}$, where $\hat{1}$ is the unit operator.

These collision cross-sections are scalar in nature, and so while they give us information on the likely outcome of a collision process, they are somewhat lacking in detailed dynamical or mechanistic information. Such information is instead best obtained from vector properties, describing (for example) the role of the reactant spatial polarisation or the conformation of the colliding particles and their detailed relative motions. The differential cross-section is particularly useful in this regard; quantifying the scattering angle dependence of the integral cross-section gives a highly detailed insight into the collision dynamics, and its interpretation is appealingly intuitive.[25,26] By transforming from the spherical wave basis to a plane wave basis, the state-to-state resolved differential cross-section can be written in terms of the helicity frame $\hat{T}$-matrix elements as

$$\frac{\mathrm{d}\sigma}{\mathrm{d}\omega}_{j'k'jk}(\theta) = \frac{4\pi^2}{k_{\text{vec}}^2} \left| \sum_J \frac{2J+1}{4\pi} d^J_{k'k}(\theta) \langle j'k'|\hat{T}^J|jk\rangle \right|^2, \qquad (2)$$

where $d^J_{k'k}(\theta)$ is a reduced Wigner rotation matrix element.[27] In this work, the collision geometry is defined such that the H_2 molecule lies at the origin of the space fixed frame, with the atomic partner's relative velocity directed along the $+Z$ axis. The scattering angle θ is then given by the polar angle of the outgoing scattered HF or HD diatom, as shown in Fig. 1. As such, forward scattering ($\theta = 0$) corresponds to the HF or HD product molecule travelling in the same direction as the initial F or D atom.

The above equations give an example of how the $\hat{S}$-matrix elements can be routinely manipulated to calculate observable properties of interest. In the following, we expand this analysis to consider the scattering behaviour of a coherent superposition of initial states, such as a rotational wavepacket. A rotational wavepacket under field free conditions can be written as a linear combination of its composite eigenstates as

$$|\Psi(t)\rangle = \sum_{jm} b_{jm}(t)\,|jm\rangle, \qquad (3)$$

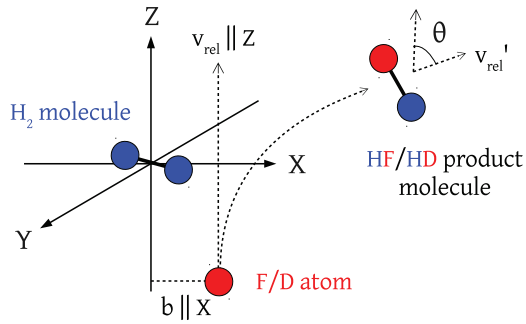

FIG. 1. Depiction of the space fixed collision frame employed in this work. The space fixed Z axis is defined by the direction of the incoming relative velocity, v_{rel}, and the space fixed X axis by the impact parameter, b. The scattering angle, θ, is defined as the polar angle of the outgoing scattered diatomic HD or HF product molecule, as depicted. Note that the scattering calculations themselves were carried out in the body fixed helicity frame, where the quantisation axis is given by the relative momentum vector.

where m is the projection quantum number of $\mathbf{j}$ onto the space fixed Z axis. The time-dependent expansion coefficients are specified by a constant value and a time-dependent phase, which varies according to

$$b_{jm}(t) = c_{jm}\ \exp\left(-i\frac{\hbar}{2I}\,j(j+1)t\right), \tag{4}$$

where I is the moment of inertia of the diatom. In the same way, the wavepacket $\hat{S}$-matrix elements can be written as a coherent superposition of the conventional eigenstate-to-eigenstate $\hat{S}$-matrix elements, such that

$$\langle j'k'|\hat{S}^{JM}|\Psi(t)\rangle = \sum_{jk} b_{jk}(t)\,\langle j'k'|\hat{S}^{JM}|jk\rangle. \tag{5}$$

Note that for the initial state (in which the incoming linear momentum lies along the $+Z$ axis), the helicity frame quantisation axis and the space fixed quantisation axis coincide exactly, and we have the convenient result $c_{jk} = c_{jm=k}$, and $|jk\rangle = |jm\rangle$. The integral cross-section is then calculated as before, yielding

$$\sigma_{j'k'\Psi(t)} = \frac{\pi}{k_{\mathrm{vec}}^2}\sum_J (2J+1)\,|\langle j'k'|T^J|\Psi(t)\rangle|^2. \tag{6}$$

The differential cross-section of a coherent superposition of eigenstates can then be written as

$$\frac{\mathrm{d}\sigma}{\mathrm{d}\omega}_{j'k'\Psi(t)}(\theta) = \frac{4\pi^2}{k_{\mathrm{vec}}^2}\left|\sum_J \frac{2J+1}{4\pi}\,d^J_{k'k}(\theta) \times \sum_{jk} b_{jk}(t)\,\langle j'k'|\hat{T}^J|jk\rangle\right|^2. \tag{7}$$

The above equations all specify the scattering dynamics of a rotational wavepacket at a particular time, t, in its evolution. As we will discuss in Subsection II B, the expansion coefficients defining the wavepacket, $b_{jk}(t)$, oscillate in phase on the timescale of the rotational period of the molecule. The varying coherences between eigenstates that give rise to a time-dependent polarisation of the wavepacket will also give rise to a similar time dependence of the scattering dynamics. This feature is fully incorporated in the above expressions.

However, in a typical scattering experiment the exact timing of the collision relative to the rotational phase of the diatom cannot be controlled. The duration of a typical molecular beam pulse has a lower limit on the order of tens of μs, many orders of magnitude higher than the rotational period, and so even if the individual collision events themselves can be considered to be instantaneous, any experimentally observed results will be averaged over the time dependence of the rotational wavepacket. In this case, it is no longer appropriate to consider the target diatom as a coherent superposition of eigenstates. The averaging over the time dependence is equivalent to an averaging out of the coherences existing between the states. In terms of the density matrix describing the wavepacket, the off-diagonal elements all average out to zero over time, while the diagonal elements remain unchanged.[28] What remains upon taking a time average is thus effectively an incoherent mixture of eigenstates that can no longer be described as a pure state. In this case, the integral cross-section is now given as

$$\sigma_{j'k'\overline{\Psi(t)}} = \frac{\pi}{k_{\mathrm{vec}}^2}\sum_J (2J+1)\sum_{jk}|c_{jk}|^2|\langle j'k'|T^J|jk\rangle|^2 \tag{8}$$

and the differential cross-section as

$$\frac{\mathrm{d}\sigma}{\mathrm{d}\omega}(\theta) = \frac{4\pi^2}{k_{\mathrm{vec}}^2}\sum_{jk}|c_{jk}|^2\left|\sum_J \frac{2J+1}{4\pi}\,d^J_{k'k}(\theta)\,\langle j'k'|\hat{T}^J|jk\rangle\right|^2 \tag{9}$$

as is appropriate for a statistical mixture of states. Comparing the scattering dynamics of the time averaged and time-dependent rotational wavepackets thus provides a precise measure of the importance of the coherences between eigenstates in determining the outcome of a collision event.

Finally, it should be noted that although we have restricted ourselves to consideration of the integral and differential cross-sections in this study, it is also perfectly possible to extend the calculation of any other scalar or vector correlation of interest[29] to include a rotational wavepacket as the initial reactant state. For example, information on the $\mathbf{j}$-$\mathbf{j}'$ vector correlation is contained within the tensor cross-sections, which are also of particular interest in determining the rate of collision induced depolarisation of a rotational wavepacket in the presence of a bath gas.[30–33] This quantity could be calculated simply by replacing the usual eigenstate-to-eigenstate $\hat{S}$ matrix elements $\langle j'k'|\hat{S}|jk\rangle$ that appear in the calculation with the appropriate coherent superposition $\langle j'k'|\hat{S}|\Psi(t)\rangle = \sum b_{jk}(t)\langle j'k'|\hat{S}|jk\rangle$ in the manner prescribed above.

B. Characterisation of laser induced rotational wavepackets

Rotational wavepackets which create alignment of the molecular bond axis can be induced with moderately intense, short laser pulses. In the case of a homonuclear diatomic molecule, there is no permanent dipole moment, and so the interaction progresses through an induced dipole, the magnitude of which is proportional to the difference in the polarisability of the molecule along its major and minor axes. For the interaction of a diatom with a linearly polarised laser pulse, the

Hamiltonian of the system can be written as[6]

$$\mathcal{H} = \frac{\hat{j}^2}{2I} - \frac{1}{4}\mathcal{E}(t)^2[(\alpha_\parallel - \alpha_\perp)\cos^2(\Theta) + \alpha_\perp], \qquad (10)$$

where $\alpha_\parallel$ and $\alpha_\perp$ are the polarisabilities of the molecule parallel and perpendicular to the bond axis, respectively, $\mathcal{E}(t)$ is the intensity profile of the laser pulse as a function of time, and Θ is the angle between the bond axis and the polarisation direction of the electric field. The wavefunction of the system after excitation can be expanded as a series of composite eigenstates, as detailed in Eqs. (3) and (4). For a given initial state $|\Psi(t{=}0)\rangle = |j_0 m_0\rangle$, the coefficients $b_{jm}(t)$ are obtained by numerically solving the time-dependent Schrödinger equation. Note that the initial magnetic quantum number m_0 is preserved during the interaction with the laser pulse, so that $b_{jm}(t) = b_{jm_o}(t) = b_j(t)$ when the electric vector of the excitation laser lies parallel to the space fixed Z axis. Moreover, the parity of the rotational states is conserved, i.e., for an initial state with even (odd) j only even (odd) rotational states are excited.

After the interaction, the rotational wavepacket evolves freely, allowing us to write

$$|\Psi(\tau)\rangle = \sum_j c_j \exp(-ij(j+1)\tau)\,|jm_0\rangle, \qquad (11)$$

where $c_j = b_j(\tau_{\text{end}})$ are the values of the expansions coefficients at the end of the interaction period, and where we have made use of the dimensionless time variable $\tau = t\hbar/2I$. Once formed, the rotational wavepacket exhibits a rich variety of time-dependent dynamical behaviour, cycling through various states of polarisation throughout the rotational period of the diatom as the coherences between the composite eigenstates evolve. The degree of alignment of the molecular bond axis along the electric vector axis is measured by the time-dependent alignment factor $\langle\cos^2\theta\rangle$, related to the alignment polarisation moment $a_0^2 = \langle P_2(\cos(\theta))\rangle$ where P_n is the nth order Legendre polynomial. In the experimentally realistic case where a thermal distribution of rotational states exist prior to the arrival of the excitation laser beam, each thermally populated $|j_0 m_0\rangle$ state will effectively give rise to its own characteristic wavepacket. The resulting total state of the target diatom is then best described as a statistical mixture of this collection of coherent wavepacket states, weighted by the thermal populations of the precursor eigenstates.

Fig. 2 depicts the well-known time-dependent alignment of such a rotational wavepacket, formed from a thermal rotational distribution at 200 K of p-H_2 (red) and o-H_2 (blue), using a single instantaneous laser pulse of reduced pulse strength $P = 10$. The reduced pulse strength is defined as[34,35]

$$P = (\alpha_\parallel - \alpha_\perp)\, I \int \mathcal{E}(t)^2/(4\hbar^2)\,\mathrm{d}t. \qquad (12)$$

For the H_2 molecule, a reduced pulse strength of $P = 10$ corresponds to an intensity of 1.2×10^{14} W/cm^2 over a laser pulse characterised by a Gaussian time profile with a FWHM of 20 fs.

Note that in Fig. 2, a value of $\langle\cos^2(\theta)\rangle = 1/3$ implies a perfectly unaligned distribution, while the upper and lower limiting values of one and zero correspond to perfect alignment and anti-alignment along the laser electric vector axis, respectively. In the absence of any decoherence of the wavepacket, the pattern over the 2π interval of the reduced time variable is repeated indefinitely. For the H_2 molecule, the 2π interval of the reduced time variable τ corresponds to a time of around 500 fs.

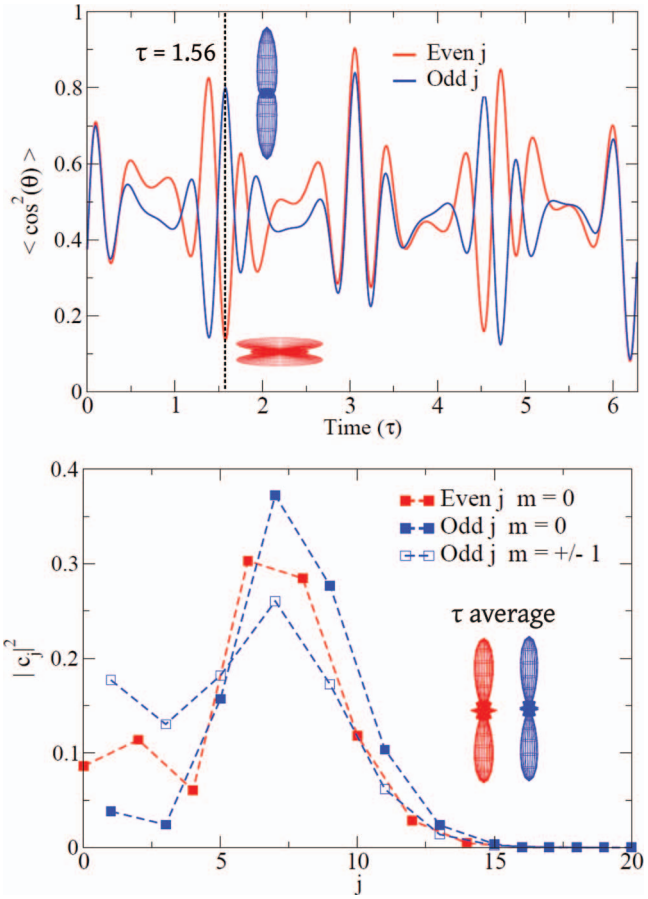

FIG. 2. The upper panel shows the time-dependent alignment factors for the rotational wave packets formed from p-H_2 (in red) and o-H_2 (in blue), using a single instantaneous laser pulse of reduced pulse strength $P = 10$ and an initial rotational temperature of 200 K. The lower panel depicts the square modulus of the expansion coefficients defining the wavepackets originating from the most strongly populated states, $|j_0 = 0, m_0 = 0\rangle$, (in red), $|j_0 = 1, m_0 = 0\rangle$ (solid blue points), and $|j_0 = 1, m_0 = \pm 1\rangle$ (open blue points), in the initial thermal distribution. Plots of the bond axis probability distributions for o-H_2 and p-H_2 are shown at a fixed time of $\tau = 1.56$, corresponding to 123 fs (upper panel), and averaged over the revival period of the wavepacket (lower panel). The space fixed Z axis is aligned vertically.

Although the *time averaged* alignment of the o-H_2 and p-H_2 wavepackets is similar, it can be seen that the time-dependent alignment factor for the two wavepackets oscillates rapidly, and in opposite senses for the two nuclear spin modifications. A graphical depiction of the bond axis angular distributions is displayed at $\tau = 1.56$, which corresponds to 123 fs (in the upper panel of Fig. 2), along with the corresponding time averaged distributions (in the lower panel). The absolute values of the expansion coefficients of the various rotational states can be seen to be similar for both wavepackets, as shown in the lower panel of Fig. 2. Nevertheless, the time-dependent angular distributions differ dramatically from one another, underlining the importance of the coherences

between rotational states. It should also be emphasised at this stage that this polarisation is of a fundamentally different character than that usually encountered in polarised scattering experiments. One would usually associate an anti-aligned state with the magnetic quantum number $m = j$, but in this case the polarisation arises entirely from interference between the populated rotational levels, with only a single value of m (usually with $m \ll j$) being populated in each wavepacket. Previous studies of alignment effects in gas phase scattering have largely been restricted to coherences between the different magnetic sub-levels,[29,36,37] and as such are highly complementary to the approach considered in this work, where it is the coherences between the different j levels that give rise to the molecular alignment.

By judiciously choosing a particular time within the evolution of the wavepacket at which to fire in one or more subsequent laser pulses, the composition and behaviour of the wavepacket can be customised to a large degree. In this manner, schemes have been developed to achieve time-dependent polarisations that approach their theoretical upper and lower limits, and to obtain wavepackets which are permanently either positively or negatively aligned with respect to the laser electric field axis, even after the electric field is switched off.[38] Alternatively, sophisticated choices of laser pulse can be employed to create a uni-directionally rotating wavepacket.[39,40] Such methods offer appealing possibilities for fine control of the initial state of a collision system prior to an investigation of its scattering dynamics. In this study, we also consider a third application, parity selective control over the degree of rotational excitation of the wavepacket.[10,41]

As an example, Fig. 3 shows the effect of a second laser pulse scheme designed to rotationally excite the p-H_2 wavepacket while suppressing the rotation of the o-H_2 wavepacket, as demonstrated, for example, in Ref. 10. Here, a first pulse of reduced strength $P = 5$ is followed by a second pulse with a higher strength of $P = 15$ at the reduced time $\tau = 4.55$. As can be seen, the resulting p-H_2 rotational population distribution is shifted towards higher rotational states, while the o-H_2 wavepacket rotation is suppressed. This is achieved by timing the second pulse so that the phase of the p-H_2 molecules is such that they are rotating in the same direction as the "kick" given by the laser pulse, effectively speeding up their rotation. Conversely, the phase of the o-H_2 molecules is such that they are rotating in the opposite direction, so that their rotation is impeded by the impulse imparted by the laser pulse. In addition to the strong differences in the degree of rotational excitation experienced by the two wavepackets, the high j wavepacket of p-H_2 also exhibits a stronger positive alignment than the low j wavepacket of o-H_2, due to the increased capacity for polarisation as j increases.

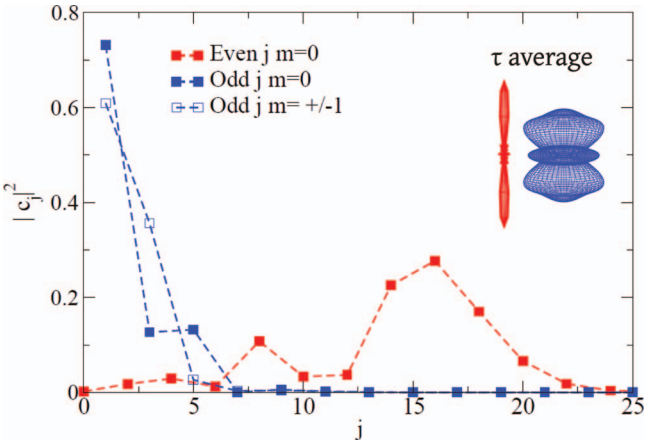

FIG. 3. Rotational population distributions for wavepackets of p-H_2 (in red) and o-H_2 (in blue) formed by the application of the two pulse laser excitation scheme discussed in the text to the most strongly populated states, $|j_0 = 0, m_0 = 0\rangle$, (in red), $|j_0 = 1, m_0 = 0\rangle$ (solid blue points), and $|j_0 = 1, m_0 = \pm 1\rangle$ (open blue points), in an initial rotational temperature of 200 K. Time averaged bond axis probability distributions are also plotted for o-H_2 and p-H_2. The space fixed Z axis is aligned vertically.

The ability to selectively control the rotational populations of different nuclear spin modifications of the collision precursor in this fashion opens up an alternative avenue of applications in collision experiments, as will be investigated in the Sec. III B.

It should be noted at this stage that it is generally only possible to rotationally excite a small proportion of the molecules present in a typical molecular beam pulse in this fashion. As such, it is important for a scattering experiment to be able to selectively detect only those scattering events that take place between molecules in rotational wavepacket initial states. Fortunately, the excitation efficiency within the spatiotemporal volume of the excitation laser is sufficiently high that the majority of molecules passing through this volume can be excited into rotational wavepacket states.[42] The detection laser can then be fired into the same volume after some short delay (of the order 100 ns). This time delay should be chosen to allow a suitable interval for collisions to occur, within which the molcules will travel only a short distance compared to the size of the excitation volume. This ensures that only those molecules that were originally in the excitation volume will be detected. Thus selective detection of only those molecules which were initially present in the excitation volume is achieved.

This method has been successfully employed in the observation of the differential cross section of electronically excited NO(A) with Ar and He.[43] In our case, the detection laser(s) will ionise molecules in a particular product ro-vibrational state regardless of whether or not the molecule was initially in a rotational wavepacket state, giving rise to some degree of background signal. The level of this background signal will depend solely on the excitation efficiency within the excitation laser volume, which is sufficiently high that the experiment should be feasible. Additionally, when the rotational energy of the wavepacket is higher than the thermally populated eigenstates present in the molecular beam, the higher energy ro-vibrational product eigenstates can only be accessed via the rotational wavepacket. As such, detection of scattered signal in these high energy product eigenstates is guaranteed to be background free in a rigorous sense.

C. Calculation details

The quantum reactive scattering package "abc"[24] was used to generate the requisite $\hat{S}$-matrix elements for the

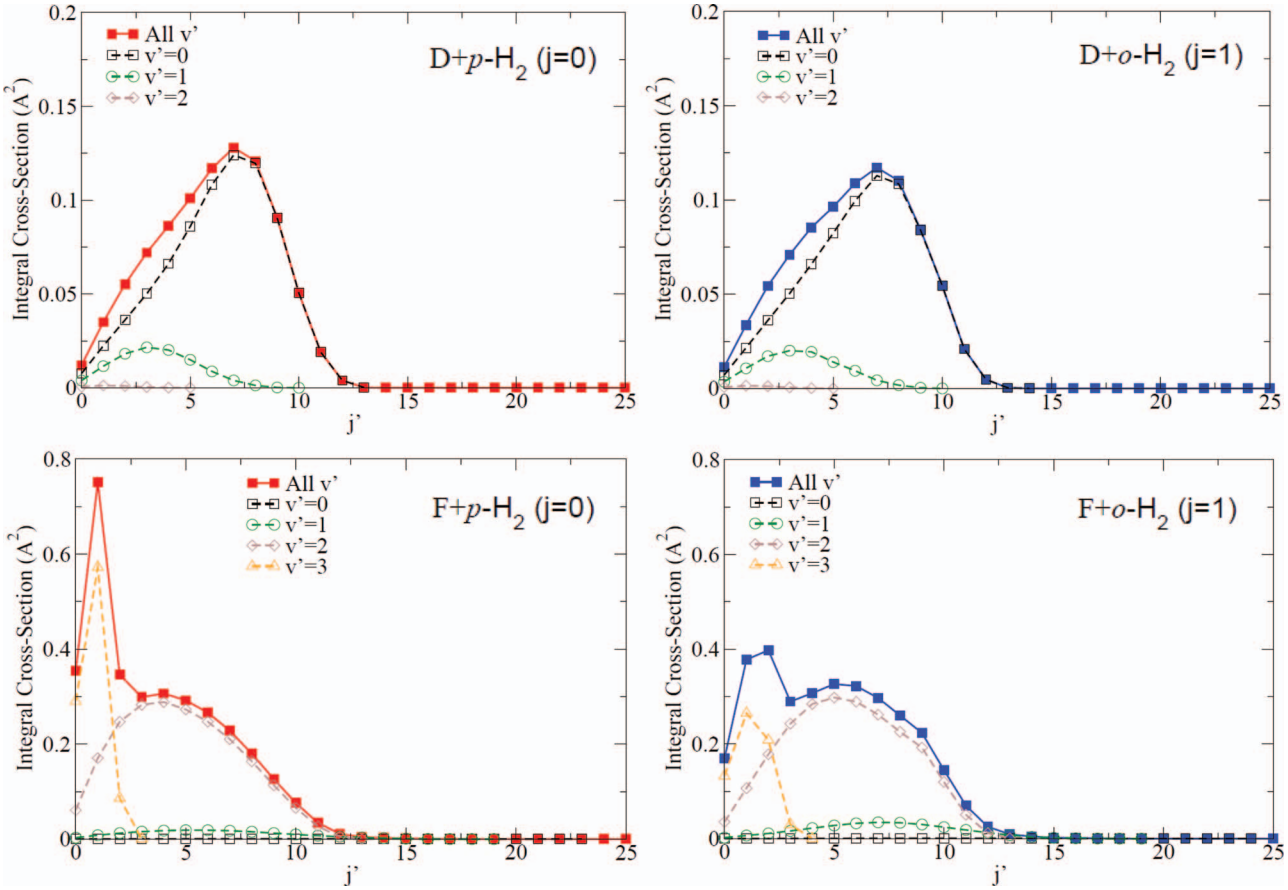

FIG. 4. Reactive final state resolved integral cross-sections for the D+H_2 (upper panels) and F+H_2 (lower panels) systems, for collision energies of 1.00 eV and 0.05 eV respectively, for the initial target eigenstates $|j = 0, m = 0\rangle$ (in red) and $|j = 1, m = 0,\pm1\rangle$ (in blue). The final vibrational and rotational states are denoted by v' and j', respectively.

reactive scattering calculations performed in this work. The Liu-Siegbahn-Truhlar-Horowitz (LSTH) PES[44–46] was used for the calculations on D+H_2, and the Stark-Wener (SW) PES[47] was employed for the F+H_2 system. Since each individual scattering calculation is run at a fixed *total* energy, each different initial rotational quantum state is associated with a different *collision* energy. For this reason, it was necessary to run a separate scattering calculation for each initial rotational state, adjusting the total energy so as to obtain a constant collision energy of 1.00 eV for D+H_2 and 0.05 eV for F+H_2.

In order to converge the scattering calculations it is necessary to specify the size of the basis sets used, and the manner in which the integration of the close-coupled equations is carried out. For the D+H_2 reaction, a rotational basis up to $j = 25$ was employed, including states up to a maximum energy of 3.2 eV, and propagation was carried out up to a maximum hyper-radius of 12 bohrs, divided into 200 sectors. Partial waves up to $J = 50$ and helicity projection quantum numbers up to $k_{\max} = 5$ were included to ensure convergence of the $\hat{S}$-matrix elements. For the F+H_2 reaction, a rotational basis up to $j = 25$ was employed, including states up to a maximum energy of 3.2 eV, and propagation was carried out up to a maximum hyper-radius of 12 bohrs, using 150 sectors. Inclusion of partial waves up to $J = 30$ and helicity projection quantum numbers up to $k_{\max} = 4$ were sufficient to converge the reactive cross-sections.

Thermal averages were taken over the initially populated rotational levels of the H_2 molecule prior to the first laser pulse, assuming a rotational temperature of 200 K. This value was chosen to match the conditions in a typical experimental molecular beam of hydrogen molecules.[48] Note that this is significantly higher than the rotational temperatures typically obtained under supersonic expansion conditions; this can be attributed to the poor efficiency of rotational cooling due to the large rotational constant of the hydrogen molecule. In terms of the population of rotational levels, this temperature corresponds to around a 3:1 ratio of $j = 0$ to $j = 2$ in p-H_2 and a 30:1 ratio of $j = 1$ to $j = 3$ in o-H_2, with equal population of all m sub-levels. Calculations of the wavepacket formation and the subsequent scattering dynamics were performed for each thermally populated initial state and a weighted average was then taken over the thermal populations.

III. RESULTS

In this section, we present a case study of the reactive scattering dynamics of rotational wavepackets. The D+H_2 reaction at a collision energy of 1.00 eV and the F+H_2 reaction at a collision energy of 0.05 eV are used as model systems. The simplistic nature of these systems, and the accurate potential energy surfaces that are available for their characterisation, enable precise quantum mechanical scattering

calculations to be performed, followed by a simple mechanistic analysis of the resulting data. The isotopic variant D+H_2 is considered to allow experimental differentiation between the non-reactive H_2 molecules and the reactive HD molecules formed during the collision. For each of the two model systems, the collision dynamics of a variety of initial states are considered, exploring the range of (nuclear spin modification dependent) influence that can be exerted on the collision process.

A. Single pulse coherent (fixed time) and incoherent (time averaged) wavepacket scattering

For the purpose of comparison, we first consider conventional reactive scattering in which the target state is simply the ground rotational eigenstate of either *p*-H_2 or *o*-H_2. This represents the dominant reactive scattering dynamics that would be observed in the absence of any excitation laser pulse using a rotational temperature of 200 K. The corresponding reactive integral and total reactive differential (summed over all final product states) cross-sections for the D+H_2 and F+H_2 reactions are depicted in Figs. 4 and 5 for the ground rotational states of *p*-H_2 and *o*-H_2.

For the D+H_2 reaction, the parity of the initial state makes very little difference to the cross-sections. The only noticeable differences are the small oscillations present in the *o*-H_2 differential cross-section, which can be traced back to the $|j = 1, m = \pm 1\rangle$ initial eigenstates. In the F+H_2 reaction, the initial state $j = 0$ is relatively much more strongly forward scattered than the $j = 1$ eigenstate. This strong alternation in behaviour arises not from the parity of the initial state, but rather from the presence of resonances in the $v' = 3$ product channel of the F+H_2 reaction for the initial state $j = 0$.[49,50]

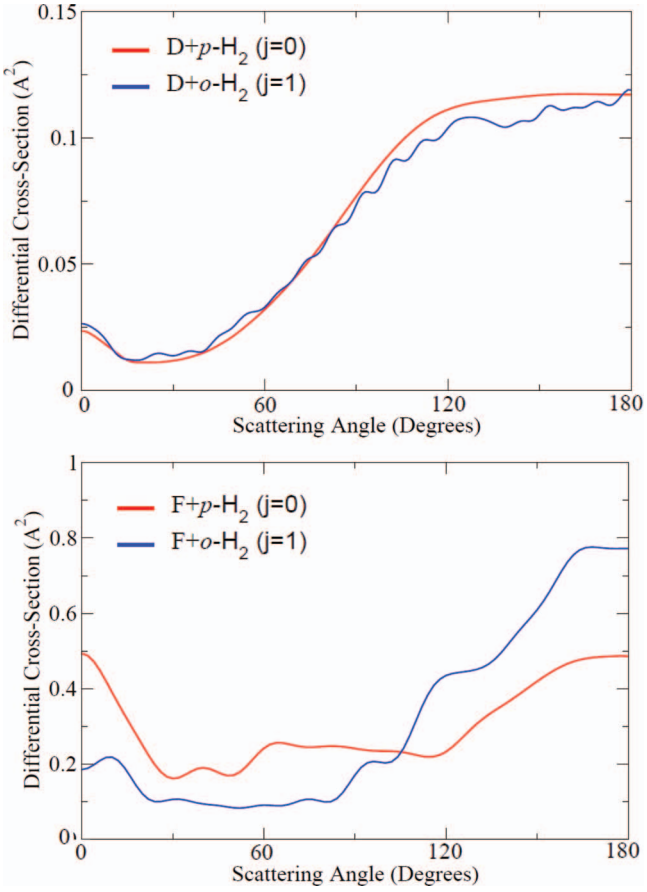

FIG. 5. Total reactive differential cross-sections for the D+H_2 (upper panel) and F+H_2 (lower panel) systems, for collision energies of 1.00 eV and 0.05 eV respectively, for the initial target eigenstates $|j = 0, m = 0\rangle$ (in red) and $|j = 1, m = 0, \pm 1\rangle$ (in blue).

The integral cross-sections of the two reactions differ more substantially, with a much more significant degree of product vibrational excitation being observed for the F+H_2 reaction. This difference reflects the strong exo-energetic nature of the F+H_2 reaction compared to the energetically neutral D+H_2 system, and the symmetric position of the transition state in the D+H_2 reaction compared to the early position of the energetic barrier in the F+H_2 system.

Due to the lack of coherences, and the equal population of all *m* magnetic sub-levels, the bond axis distribution for these initial states is spherically symmetric. Considering the dynamics of the D+H_2 reaction, the similarities between the data sets for *p*-H_2 and *o*-H_2, and the smooth, relatively featureless structure in the differential cross-section are both reflections of this spherical symmetry of the H_2 bond axis distribution prior to the scattering event. The averaging over all possible collision geometries resulting from this spherical symmetry yields little insight into the mechanism by which the two reactions progress, although the preferential backward scattering of the product diatom would suggest that relatively direct collisions are preferred over long range, grazing encounters. Previous studies have further indicated that the scattering dynamics of the D+$H_2(j = 0, 1)$ system can be largely accounted for with a simple classical lines-of-centre model.[51] As previously noted, the oscillatory structures in the differential cross-sections of the F+H_2 reaction arise from resonances in the $v' = 3$ product channel rather than from bond axis polarisation effects.[49,50]

Conventional reactive scattering from a spherically symmetric ensemble of eigenstates is in stark contrast to the strongly polarised bond axis distributions that can be created with short laser pulses. Therefore, we now move on to consider the scattering dynamics associated with a coherent, polarised, rotational wavepacket initial state. As a first case, we consider the coherent wavepacket state depicted for $\tau = 1.56$ in Fig. 2. A single laser pulse of reduced pulse strength $P = 10$ is used to coherently excite rotational levels in the range $0 < j < 15$ from an initial rotational thermal distribution at 200 K, and the resulting wavefunction at the fixed reduced time point $\tau = 1.56$ is then employed as the reactant in the scattering calculation.

It should be noted at this stage that the time resolved situation assumed here is not experimentally achievable, since in reality the duration of the molecular beam pulses employed in scattering experiments are many orders of magnitude larger than the oscillatory behaviour of the wavepacket. Nevertheless, it provides a useful case to investigate before turning our attention to more realistic scenarios.

Figs. 6 and 7 depict the integral and the total differential reactive cross-sections for the D+H_2 and F+H_2 reactions, where the reactant quantum state is given by the wavefunction

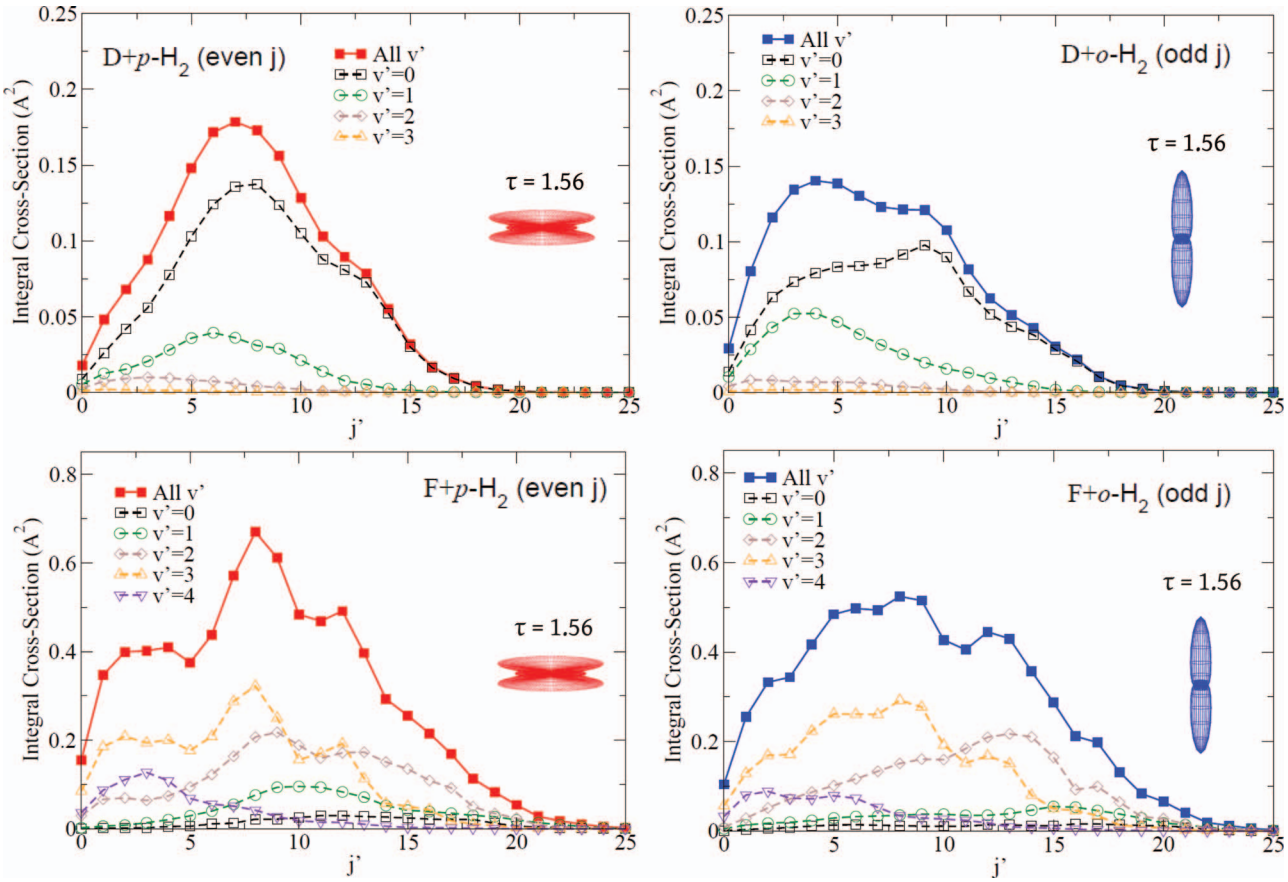

FIG. 6. Reactive final state resolved integral cross-sections for the D+H_2 (upper panels) and F+H_2 (lower panels) systems. The initial coherent rotational wavepacket state for p-H_2 (in red) and o-H_2 (in blue) is created using a single laser pulse as described in the text and in Figure 2. The final vibrational and rotational states are denoted by v' and j', respectively. Angular bond axis probability distributions are shown in the insets, where the incoming relative velocity, $v_{\rm rel} \| Z$ is aligned vertically.

specified above. Focusing first on the reactive integral cross-sections displayed in Fig. 6, we see that for the D+H_2 system, the anti-aligned p-H_2 state leads to relatively more rotational excitation, and relatively less vibrational excitation than the strongly aligned o-H_2 wavepacket. This behaviour can be rationalised in terms of a purely classical picture; collisions associated with the strongly aligned o-H_2 wavepacket will tend to take place in a head-on linear configuration leading to vibrational excitation, while collision of the p-H_2 molecules will favour more glancing T-shaped configurations, leading to rotational excitation.

As can be seen in Fig. 7, the total reactive differential cross-sections for the D+H_2 reaction also depend strongly on the polarisation of the reactant wavepacket, and hence on the parity of the nuclear spin wavefunction. In both cases the angular probability distributions differ substantially from the spherically symmetric initial eigenstate targets considered previously, highlighting the importance of the coherence induced polarisation in determining the outcome of the scattering process. Sideways scattered collisions are favoured for the positively aligned o-H_2 wavepacket, while backward scattered collisions are preferred for the anti-aligned p-H_2 wavepacket. At first glance, this result might appear somewhat surprising. For strongly aligned target molecules, one would normally expect direct collisions at small impact parameters, which will be tend to be backward scattered, while anti-aligned target molecules will be associated with larger impact parameter "glancing" blow collisions which are more likely to be sideways or forward scattered. It should be noted, however, that this conventional picture is only applicable to the familiar case where the target diatom exists in a well defined rotational eigenstate. For such eigenstates, the polarisation of the molecular bond axis is well known, but the phase of the rotational motion is unspecified, so that the molecule is equally likely to reside at any point along its orbit. In the case presented in Fig. 7, by picking a particular time point in the evolution of the coherent rotational wavepacket, we have effectively fixed the phase of the rotational motion of the diatom. This allows us to identify the direction in which the hydrogen atoms are rotating, as well as specifying their collective polarisation. The aligned rotational wavepacket is defined such that the reactant hydrogen atoms must be moving roughly perpendicular to the Z axis, as shown by the blue arrows on the plot of the o-H_2 bond axis polarisation in Fig. 7. When the collision occurs this momentum is transferred to the product diatom, biasing the formation of sideways scattered products. In the case of the anti-aligned wavepacket, the two hydrogen atoms will be moving along the $\pm Z$ axis at the time of collision, as shown by the red arrows on the corresponding p-H_2 bond axis distribution in

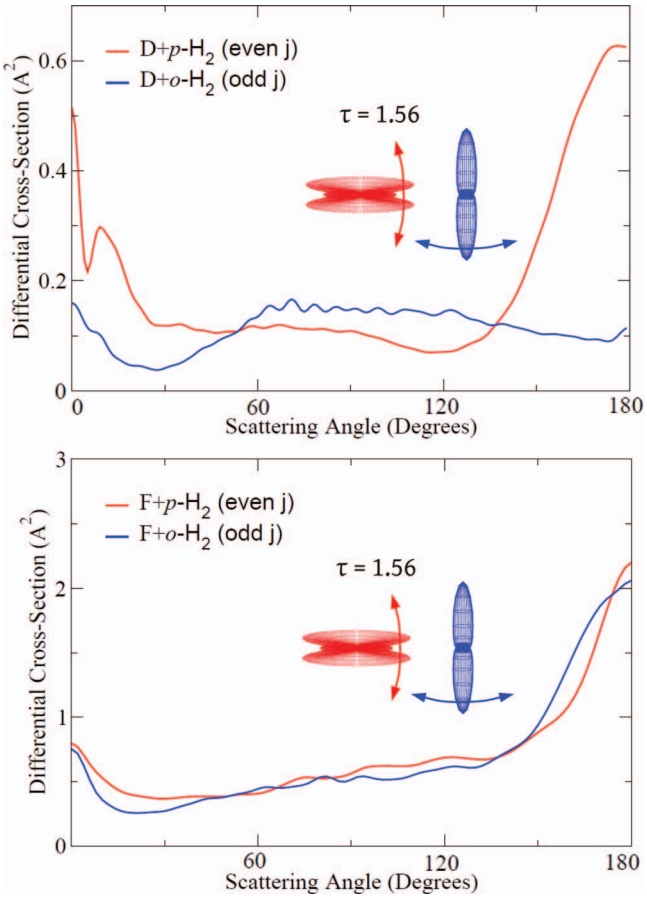

FIG. 7. Total reactive differential cross-sections for the D+H_2 (upper panels) and F+H_2 (lower panels) systems. The initial coherent rotational wavepacket state for p-H_2 (in red) and o-H_2 (in blue) is created using a single laser pulse as described in the text and in Figure 2. Angular bond axis probability distributions are shown in the insets (together with the direction of rotational motion), where the incoming relative velocity, $v_{\mathrm{rel}} \| Z$ is aligned vertically.

Fig. 7. Once again this momentum is transferred to the product molecule, giving rise to a preference for scattering in the forward and backward directions.

It should be noted that if one were to choose a different time point in the evolution of the rotational wavepackets, for which the p-H_2 wavepacket was aligned and the o-H_2 wavepacket was anti-aligned, then the dynamical behaviour is reversed. This clearly demonstrates that it is the polarisation of the initial bond axis distribution that determines the collision dynamics, which is independent of the parity of the H_2 wavepacket.[17]

Interestingly, the differences in reactivity between p-H_2 and o-H_2 is only much more weakly observed for the F+H_2 reaction. The distribution of product final states (Fig. 6) and the angular distribution of scattered products (Fig. 7) can be seen to be virtually independent of the polarisation of the H_2 molecule prior to the collision. The differences in behaviour between the two reactive systems can be attributed to several factors. The interaction potentials differ significantly, the asymmetric F+H_2 potential being strongly exo-energetic in the reactive channel, while the symmetric D+H_2 potential is energetically neutral in the reactive channel. Although this effect is countered somewhat by the choice of collision energies of 1.00 eV for D+H_2 and 0.05 eV for F+H_2, the F+H_2 reaction leads to a significantly higher degree of vibrational excitation in the HF product molecule than is observed for the HD product molecules in the D+H_2 reaction. Perhaps most importantly, the D+H_2 reaction progresses through a relatively tightly constrained linear transition state,[51] while the F+H_2 reaction passes through a less stringent bent intermediate.[52,53] This will clearly affect the preferred relative orientation of the reactants prior to collision and is most likely the dominant factor in determining the different behaviour observed in the D+H_2 and F+H_2 systems. Essentially, the F+H_2 reaction coordinate is such that the reaction tends to progress through a similar intermediate whether the initial conditions are linear or T-shaped in nature, hence the similarity between the collision dynamics of the anti-aligned p-H_2 and the aligned o-H_2 rotational wavepackets.

As discussed previously, the duration of the molecular beam pulses employed in scattering experiments is such that the detailed time-dependent structure of the target rotational wavepacket state will be completely averaged out. In this case, the coherences between the various rotational levels cease to be of relevance and the coherent wavepacket can be replaced by an incoherent statistical mixture of the populated rotational states. The integral and total reactive differential cross-sections corresponding to this scenario are shown in Figs. 8 and 9. The initial wavepacket was prepared in the same manner as described previously, and then averaged over the 2π interval of the reduced time variable. This has the effect of removing the differences between the polarisations of the p-H_2 and o-H_2 wavepackets so that both wavepackets display a time averaged positive alignment, as shown in the plots of the bond axis probability distributions. While this has little effect on the F+H_2 reactive cross-sections, the D+H_2 reactive integral, and particularly the differential cross-sections are clearly significantly altered such that the difference between the p-H_2 and o-H_2 initial wavepackets disappears.

On closer inspection, the D+H_2 reactive integral and differential cross-sections can be seen to be given by an average of the p-H_2 and o-H_2 data presented in Figs. 6 and 7. This behaviour can be rationalised by considering that the data in Figs. 6 and 7 correspond to the maximally aligned and anti-aligned bond axis polarisations, while the data presented in Figs. 8 and 9 correspond to the time averaged polarisation. Just as the time averaged polarisation lies between the two extremes, so the time averaged integral and differential cross-sections lie between the extreme aligned and anti-aligned cases.

An alternative rationalisation for the shape of the differential cross-section can be arrived at by considering the (incoherent) contributions made by the individual $|j, m = 0\rangle$ states, a selection of which are plotted in Fig. 10. The total reactive differential cross-section of the incoherent, time averaged wavepacket is a weighted average of a series of such components. The $m = 0$ states have been selected as these are the dominant contributors to the rotational wavepackets that we have considered. As j increases, the scattering distributions depicted in Fig. 10 shift smoothly from predominantly backward ($j = 0, 4$) to forward scattered ($j = 15$). Superimposed on this general trend is a small increase in the degree

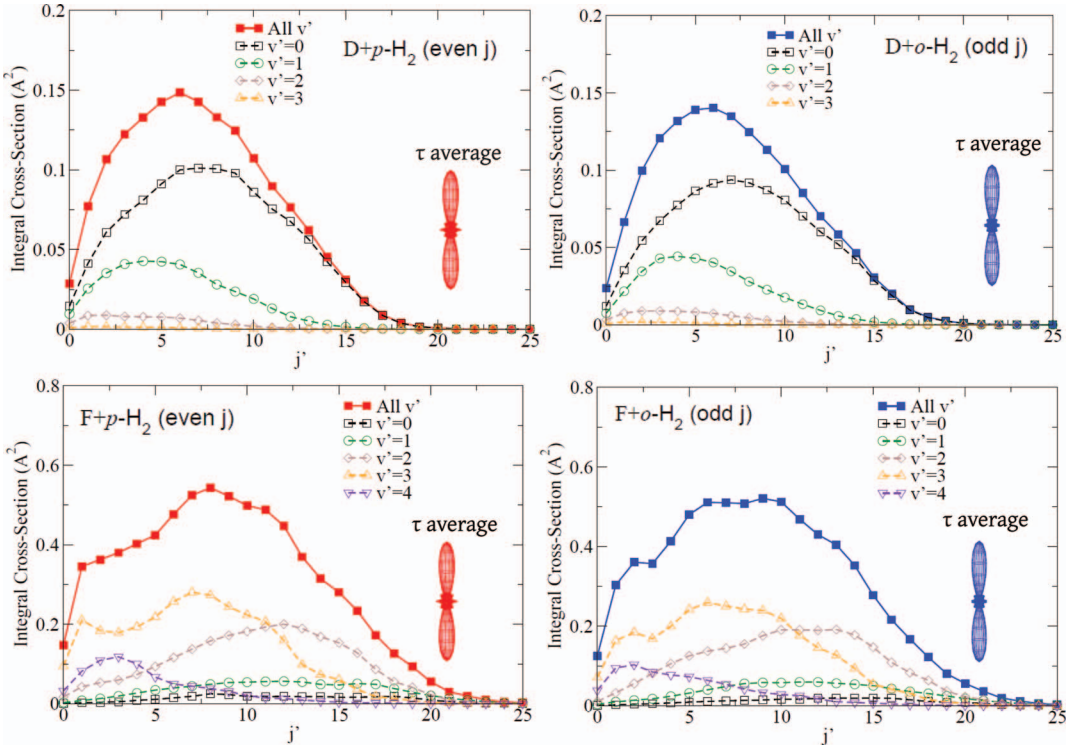

FIG. 8. Reactive integral cross-sections for the D+H_2 (upper panels) and F+H_2 (lower panels) systems. The initial coherent rotational wavepacket state for p-H_2 (in red) and o-H_2 (in blue) is created using a single laser pulse as described in the text and in Figure 2, and then averaged over the entire 2π range of the reduced time variable. The final vibrational and rotational states are denoted by v' and j', respectively. Angular bond axis probability distributions are shown in the insets, where the incoming relative velocity, $v_{\mathrm{rel}} \| Z$ is aligned vertically.

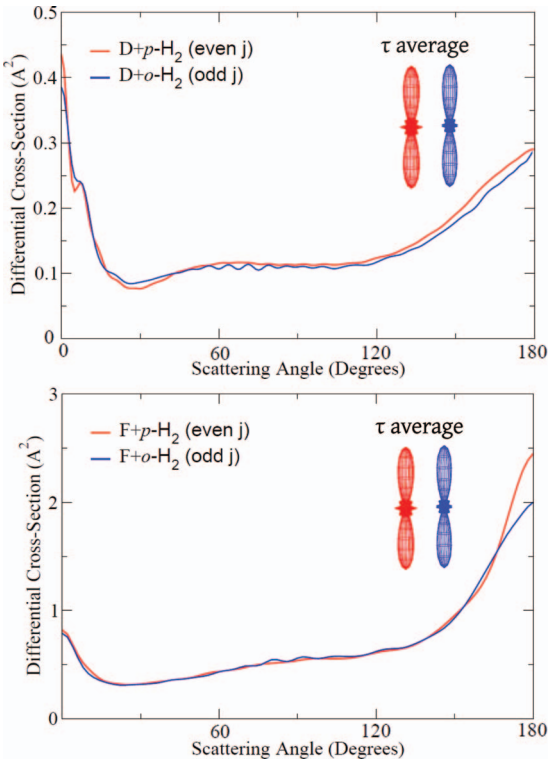

FIG. 9. Total reactive differential cross-sections for the D+H_2 (upper panel) and F+H_2 (lower panel) systems. The initial coherent rotational wavepacket state for p-H_2 (in red) and o-H_2 (in blue) is created using a single laser pulse as described in the text and in Figure 2, and then averaged over the entire 2π range of the reduced time variable. Angular bond axis probability distributions are shown in the insets, where the incoming relative velocity, $v_{\mathrm{rel}} \| Z$ is aligned vertically.

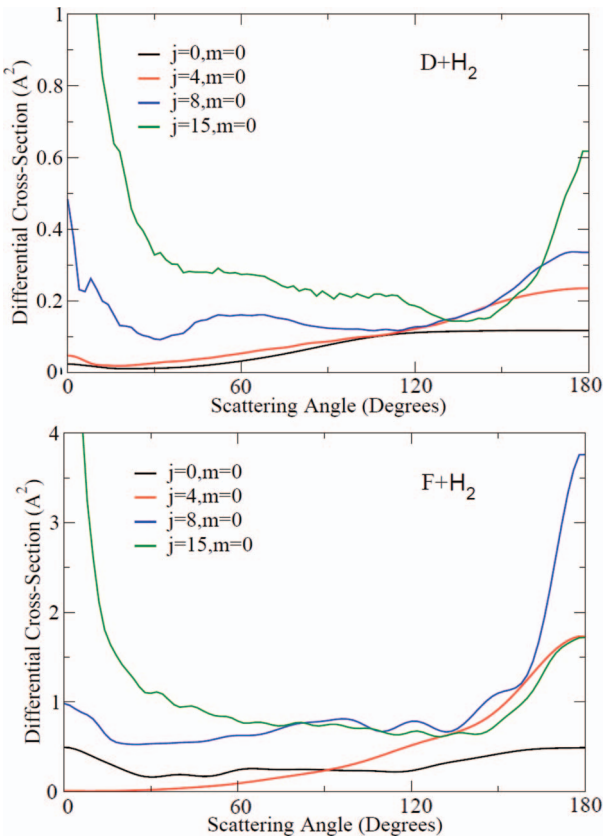

FIG. 10. Total reactive differential cross-sections for the D+H_2 (upper panel) and F+H_2 (lower panel) systems, for the initial target eigenstates $|j=0, m=0\rangle$ (in black), $|j=4, m=0\rangle$ (in red), $|j=8, m=0\rangle$ (in blue), and $|j=15, m=0\rangle$ (in green).

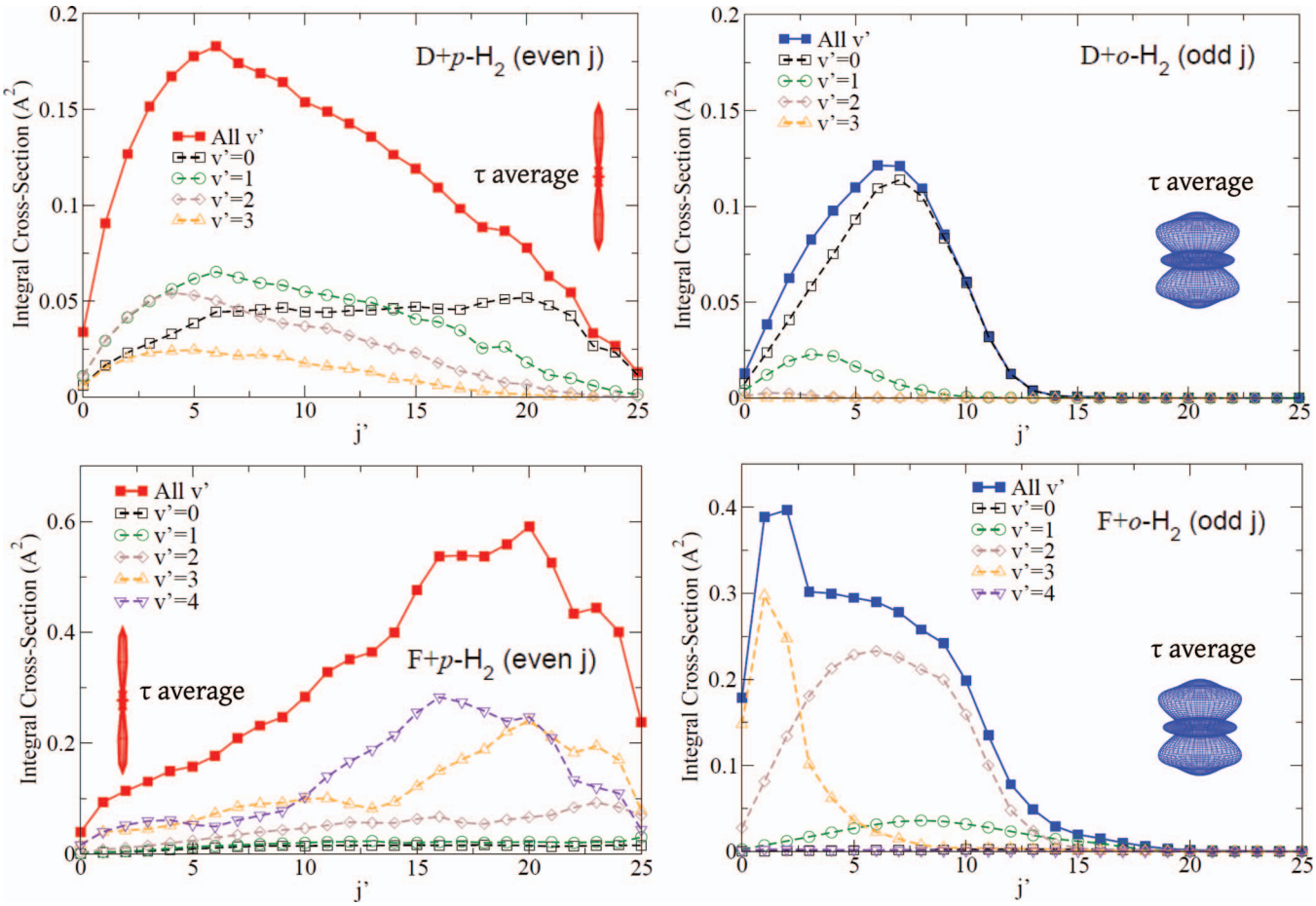

FIG. 11. Reactive integral cross-sections for the D+H_2 (upper panels) and F+H_2 (lower panels) systems. The initial coherent rotational wavepacket state for p-H_2 (in red) and o-H_2 (in blue) is created using a pair of laser pulses as described in the text and in Figure 3, and then averaged over the entire 2π range of the reduced time variable. The final vibrational and rotational states are denoted by v' and j', respectively. Angular bond axis probability distributions are shown in the insets, where the incoming relative velocity, $v_{\mathrm{rel}} \| Z$ is aligned vertically.

of backward scattering on going from $j = 0$ to $j = 4$. Note that the same trends, though less pronounced, are observed if all the m states are considered and an isotropic distribution of the H_2 bond axis is employed. In the D+H_2 reaction, the initial increase in backward scattering on going from $j = 0$ to $j = 4$ is due to the increasingly strong alignment of the H_2 molecule. This tends to favour increasingly direct collisions, which themselves tend to be increasingly backward scattered. In the F+H_2 reaction, the increased forward scattering of the initial state $j = 0$ is instead associated with quantum mechanical resonances in the $v' = 3$ product channel. As j increases further the total amount of available energy rises sharply, and reactive collisions become possible under increasingly glancing blows, which themselves correspond to the increased tendency for forward scattering observed at the higher values of j. Although in this case we are increasing the rotational energy of the reactant by increasing j, in general it has been observed that the progression from backwards to forwards scattering follows the increase in the total available energy,[54] i.e., we would observe the same shift from backwards to forwards scattering if we fixed the rotational energy and increased the collision energy instead.

The population distribution of rotational states, $|c_j|^2$, for both p-H_2 and o-H_2 contains mainly states between $j = 5$ and $j = 10$, as can be seen in the lower panel of Fig. 2. For the D+H_2 reaction, scattering from these initial states already begins to exhibit pronounced forward scattering, the signature of which can be observed in Fig. 7 for both nuclear spin modifications. For the F+H_2 reaction, on the other hand, these rotational eigenstates are still predominantly backward scattered. As a consequence, the F+H_2 differential cross-sections for the time-averaged wavepacket in Fig. 7 display no peak in the forward scattered direction, and increase monotonically in the backward scattered direction.

On going from the idealised simple case presented in Figs. 6 and 7 to an experimentally realistic case as shown in Figs. 8 and 9, it is clear that many of the interesting nuances of the reaction dynamics are lost. In Sec. III B, we consider an experimentally realistic scheme in which the differences in reactivity of the p-H_2 and o-H_2 molecules remain clearly visible even after such averaging over the revival period of the wavepacket has taken place.

B. Double pulse incoherent (time averaged) wavepacket scattering

The double laser pulse scheme discussed in Sec. II B provides just such a means to independently selectively control

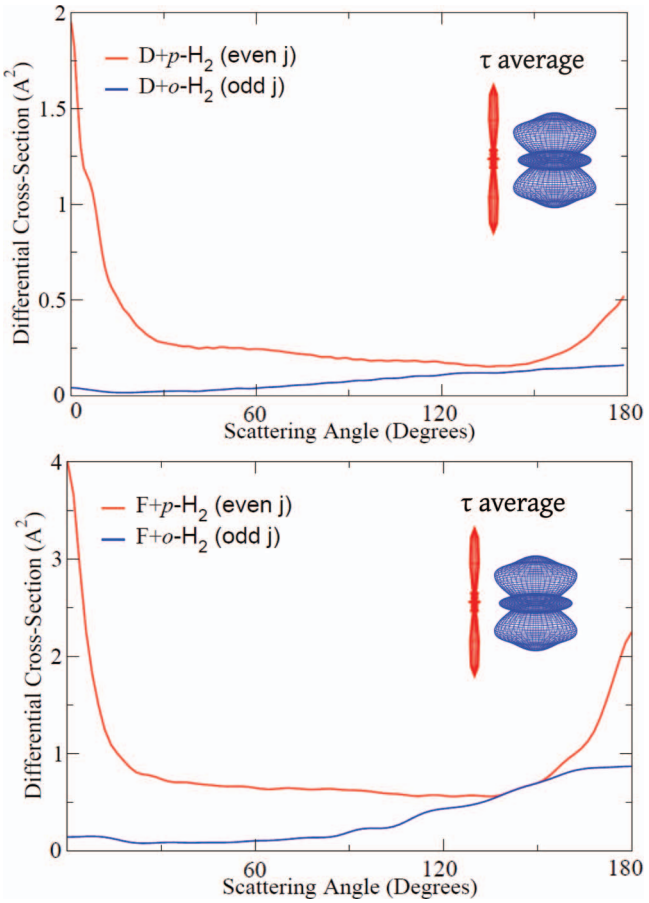

FIG. 12. Total reactive differential cross-sections for the D+H_2 (upper panel) and F+H_2 (lower panel) systems. The initial coherent rotational wavepacket state for p-H_2 (in red) and o-H_2 (in blue) is created using a pair of laser pulses as described in the text and in Figure 3, and then averaged over the entire 2π range of the reduced time variable. Angular bond axis probability distributions are shown in the insets, where the incoming relative velocity, $v_{\mathrm{rel}} \| Z$ is aligned vertically.

the rotational populations of the p-H_2 and o-H_2 wavepackets, making it eminently suitable for use under realistic experimental conditions. Starting with a thermal distribution of rotational states at 200 K, an initial laser pulse of reduced strength $P = 5$ is followed by a second pulse of strength $P = 15$ at the reduced time $\tau = 4.55$, giving rise to the distribution of rotational states depicted in Fig. 3. The corresponding integral and total reactive differential cross-sections are shown in Figs. 11 and 12. In this instance, the D+H_2 and F+H_2 reactions display similar behaviour, with the same strong differences being observed between the p-H_2 and o-H_2 targets in both systems.

On implementation of the double laser pulse scheme, the integral reactive cross-sections can be seen to differ dramatically for the p-H_2 and o-H_2 wavepackets for both the D+H_2 and F+H_2 reactions. Unsurprisingly, the p-H_2 wavepacket, composed mainly of higher rotational energy levels, leads to strongly rotationally excited products, while the o-H_2 wavepacket, composed mainly of low-lying rotational energy levels, leads to a less strongly rotational excited product distribution. The increased vibrational excitation of the p-H_2 products compared to the o-H_2 case also suggests a significant degree of rotation to vibration energy transfer during the course of the reaction. This effect is relatively stronger for the F+H_2 reaction, as would be expected for a bent transition state compared to a linear one.

The disparate rotational compositions of the p-H_2 and o-H_2 wavepackets give rise to two different effects capable of influencing the angular distribution of the scattered product molecules. The polarisation of the bond axis angular distribution can be seen to be stronger for the rotationally excited p-H_2 wavepacket than for the rotationally suppressed o-H_2 wavepacket. This is simply a consequence of the increased capacity for polarisation of high rotational states. More importantly, the total amount of available energy increases as higher rotational states are populated, leading to an increased propensity for forward scattering, as discussed previously.

Once again the differential cross-section can be rationalised by considering the weighted average of the initial eigenstate differential cross-sections presented in Fig. 10. The p-H_2 wavepacket contains many excited rotational states, which become increasingly forward scattered as j increases. For the double pulse scheme considered here, the peak of the p-H_2 rotational state distribution is around $j = 16$. As can be seen in Fig. 10, both the D+H_2 and F+H_2 reactions display strong forward scattering for $|j, m = 0\rangle$ eigenstates with $j \geq 15$, and this is reflected in the total reactive differential cross-sections shown in Fig. 12. The o-H_2 wavepacket is composed mainly of low rotational states, which are individually backward scattered. These states exhibit a broader angular distribution of scattered products, more similar in appearance to the differential cross-section associated with an isotropic distribution of the ground rotational state, as shown in Fig. 5.

It is also noteworthy that for both reactions, the total reactive integral cross-section for p-H_2 is significantly larger than that for o-H_2 due to the increased amount of internal energy available, implying significantly different reaction "rates" for the p-H_2 and o-H_2 nuclear spin modifications.

In this case, the two nuclear spin modifications of the hydrogen molecule clearly exhibit vastly different reactive product state distributions, angular scattering distributions, and reactive rate constants, using an experimentally feasible two pulse excitation scheme to create the rotational wavepacket target state.

IV. CONCLUSIONS AND OUTLOOK

In this paper, we have demonstrated that the manipulation of molecules with strong, non-resonant laser pulses can be employed to steer the outcome of reactive atom-diatom scattering. The nuclear spin dependent control over the molecular bond axis alignment that is realisable using rotational wavepackets has been successfully applied to reactive scattering systems, allowing a strong degree of nuclear spin dependent influence to be exerted over the reactive dynamics.

Using fully quantum mechanical scattering calculations for the D+H_2 and F+H_2 model reactions, we have demonstrated that (for an idealised, time resolved case) the nuclear spin modification dependent polarisation of the H_2 molecule in a rotational wavepacket gives rise to strongly differing angular distributions of the scattered product and (to a lesser

extent) product final state distributions for the case of $D+H_2$, while very little dependence was displayed for $F+H_2$. The results of this test study were rationalised in terms of the linear and bent transition states of the $D+H_2$ and $F+H_2$ reactions, respectively.

Given that the revival period over which the polarisation of a rotational wavepacket evolves is typically beyond the temporal resolution achievable in a scattering experiment, we have considered the case of a time averaged rotational wavepacket, for which the effects of the nuclear spin modification dependent polarisation are almost completely averaged out. However, we demonstrate that despite this obstacle, using a very simple double laser pulse scheme, we can construct rotational wavepackets for which the outcome of the reaction process depends very strongly on the parity of the rotational wavepacket, and hence on the nuclear spin state of the hydrogen molecule.

There are many future directions of interest in which the study of scattering of rotational wavepackets can progress. Although we have exclusively considered reactive collisions, the formalisms we have presented apply equally to vibrationally and rotationally inelastic scattering, a rich and intensely studied field in its own right. It should be noted as a caveat that rotationally inelastic collisions that are nevertheless vibrationally *elastic* will display strongly elastic type collision dynamics.

Specially tailored sequences of moderately intense, non-resonant laser pulses allow the creation of rotational wavepackets with various characteristics which open novel possibilities to control the outcome of reactive scattering experiments. Multiple laser pulse schemes have been proposed which enable the formation of rotational wavepackets which possess a permanent anti-aligned bond axis distribution,[38] in contrast to the wavepackets considered in this study which all posses a time averaged positive alignment. Such schemes would allow the experimental investigation of the effect of time averaged wavepacket polarisation, which would complement the studies based on the initial wavepacket rotational state distribution proposed in this work.

Other interesting rotational wavepackets that can be created using laser pulses include uni-directionally rotating wavepackets, where the angular momentum vector can be oriented rather than aligned.[55–57] The symmetry of the collision problem can be reduced further by considering the collision of any of the above rotational wavepackets with a surface, and calculations on such systems are currently undergoing active development.[13]

A further interesting possibility is to direct the electric vector of the laser pulse exciting the rotational wavepacket along some axis other than the initial relative velocity vector associated with the collision. In this case, the azimuthal symmetry of the collision system will be broken. This gives rise to a double differential cross-section that depends on both θ and ϕ. The coherences between the magnetic sub-levels would now become as important as the coherences between the different rotational levels making up the rotational wavepacket. The formalisms presented in this paper can be trivially extended to consider such cases, which may prove to be an interesting additional area of study.

One final particularly attractive application of a rotational wavepacket based scheme for controlling the molecular polarisation prior to a collision would be the study of collision systems involving one or more ions. Conventional electromagnetic based alignment methods cannot be applied in such cases, but the laser based alignment schemes suggested here would provide an effective means to conduct experimental studies of alignment effects in the dynamics of charge transfer processes, or in the reactions of charged particles.

In summary, we have shown that fully quantum calculations of reactive scattering of rotational wavepackets can be conducted at very little extra difficulty compared to computation of the conventional eigenstate-to-eigenstate $\hat{S}$-matrix elements. Reactive scattering with rotational wavepackets offer the possibility of novel nuclear spin modification dependent control over the outcome of a variety of chemically reactive encounters.

ACKNOWLEDGMENTS

C. J. Eyles gratefully acknowledges the receipt of an Alexander von Humboldt research fellowship in support of this work. M. Leibscher is likewise grateful for her support from the DFG (Project No. LE 2138/2-1).

[1] R. D. Levine, *Molecular Reaction Dynamics* (Cambridge University Press, Cambridge, 2004).
[2] D. R. Herschbach, Angew. Chem., Int. Ed. Engl. **26**, 1221 (1987).
[3] D. H. Parker and R. B. Bernstein, Annu. Rev. Phys. Chem. **40**, 561 (1989).
[4] R. B. Bernstein, D. R. Herschbach, and R. D. Levine, J. Phys. Chem. **91**, 5365 (1987).
[5] H. Stapelfeldt and T. Seideman, Rev. Mod. Phys. **75**, 543 (2003).
[6] T. Seideman and E. Hamilton, Adv. Mol. At. Opt. Phys. **52**, 289 (2005).
[7] S. Fleischer, Y. Khordorkovsky, E. Gershnabel, Y. Prior, and I. S. Averbukh, Isr. J. Chem. **52**, 414 (2012).
[8] B. Friedrich, D. P. Pulman, and D. R. Herschbach, J. Phys. Chem. **95**, 8118 (1991).
[9] H. J. Loesch, Annu. Rev. Phys. Chem. **46**, 555 (1995).
[10] I. S. Averbukh, S. Fleischer, and Y. Prior, Phys. Rev. Lett. **99**, 093002 (2007).
[11] E. Gershnabel and I. S. Averbukh, Phys. Rev. A **78**, 063416 (2008).
[12] M. Leibscher and T. Grohmann, J. Chem. Phys. **134**, 204316 (2011).
[13] Y. Khodorkovsky, J. R. Manson, and I. S. Averbukh, Phys. Rev. A **84**, 053420 (2011).
[14] I. S. Averbukh and E. Gershnabel, Phys. Rev. Lett. **104**, 153001 (2010).
[15] I. S. Averbukh and E. Gershnabel, Phys. Rev. A **82**, 033401 (2010).
[16] M. Quack, Mol. Phys. **34**, 477 (1977).
[17] M. Quack, J. Chem. Phys. **82**, 3277 (1985).
[18] D. Gerlich, J. Chem. Phys. **92**, 2377 (1990).
[19] M. Cordonnier, D. Uy, R. M. Dickson, K. E. Kerr, Y. Zhang, and T. Oka, J. Chem. Phys. **113**, 3181 (2000).
[20] T. Oka, J. Mol. Spectrosc. **228**, 635 (2004).
[21] A. M. Arthurs and A. Dalgarno, Proc. R. Soc. London **256**, 540 (1960).
[22] HIBRIDON is a package of programs for the time-independent quantum treatment of inelastic collisions and photodissociation written by M. H. Alexander, D. Manolopoulos, H.-J. Werner, and B. Follmeg, with contributions by P. F. Vohralik, D. Lemoine, G. Corey, R. Gordon, B. Johnson, T. Orlikowski, A. Berning, A. D. Esposti, C. Rist, P. Dagdigian, B. Pouilly, G. van der Sanden, M. Yang, F. de Weerd, S. Gregurick, and J. Kłos.
[23] M. H. Alexander and D. E. Manolopoulos, J. Chem. Phys. **86**, 2044 (1987).
[24] D. Skouteris, J. F. Castillo, and D. E. Manolopoulos, Comput. Phys. Commun. **133**, 128 (2000).
[25] C. J. Eyles, M. Brouard, C.-H. Yang, J. Kłos, F. J. Aoiz, A. Gijsbertsen, A. E. Wiskerke, and S. Stolte, Nat. Chem. **3**, 597 (2011).
[26] J. Jankunas, R. N. Zare, F. Bouakline, S. C. Althorpe, D. Herraez-Aguilar, and F. J. Aoiz, Science **336**, 1687 (2012).
[27] R. N. Zare, *Angular Momentum* (Plenum, New York, 1988).

[28]K. Blum, *Density Marix Theory and Applications* (Plenum, New York, 1996).
[29]M. P. de Miranda and D. C. Clary, J. Chem. Phys. **106**, 4509 (1997).
[30]P. Dagdigian and M. H. Alexander, J. Chem. Phys. **130**, 094303 (2009).
[31]P. Dagdigian and M. H. Alexander, J. Chem. Phys. **130**, 164315 (2009).
[32]P. Dagdigian and M. H. Alexander, J. Chem. Phys. **130**, 204304 (2009).
[33]M. Brouard, H. Chadwick, Y.-P. Chang, C. J. Eyles, F. J. Aoiz, and J. Kłos, J. Chem. Phys. **135**, 084306 (2011).
[34]M. Leibscher, I. S. Averbukh, and H. Rabitz, Phys. Rev. Lett. **90**, 213001 (2003).
[35]M. Leibscher, I. S. Averbukh, and H. Rabitz, Phys. Rev. A **69**, 013402 (2004).
[36]M. B. Krasilnikov, R. S. Popov, O. Roncero, D. D. Fazio, and S. Cavalli, J. Chem. Phys. **138**, 244302 (2013).
[37]G. G. Balint-Kurti and O. S. Vasyutinskii, J. Phys. Chem. A **113**, 14281 (2009).
[38]M. Lapert, E. Hertz, S. Guérin, and D. Sugny, Phys. Rev. A **80**, 051403(R) (2009).
[39]G. Pérez-Hernández, A. Pelzer, L. González, and T. Seideman, New J. Phys. **12**, 075007 (2010).
[40]I. V. Litvinyuk, C. T. Hebeisen, N. Kajumba, J. B. Bertrand, H. J. Worner, M. Spanner, D. M. Villeneuve, and P. B. Corkum, Phys. Rev. Lett. **109**, 113901 (2012).
[41]C. Wu, G. Zeng, Y. Gao, N. Xu, L. Peng, H. Jiang, and Q. Gong, J. Chem. Phys. **130**, 231102 (2009).
[42]E. Frumker, K. F. Lee, P. W. Dooley, D. M. Rayner, D. M. Villeneuve, and P. B. Corkum, Phys. Rev. Lett. **90**, 233003 (2003).
[43]J. J. Kay, J. D. Steill, J. Klos, G. Paterson, M. L. Costen, K. E. Strecker, K. G. McKendrick, M. H. Alexander, and D. W. Chandler, Mol. Phys. **110**, 1693 (2012).
[44]S. Siegbahn and B. Liu, J. Chem. Phys. **68**, 2457 (1978).
[45]D. G. Truhlar and C. J. Horowitz, J. Chem. Phys. **68**, 2466 (1978).
[46]D. G. Truhlar and C. J. Horowitz, J. Chem. Phys. **71**, 1514 (1979).
[47]K. Stark and H.-J. Werner, J. Chem. Phys. **104**, 6515 (1996).
[48]C.-H. Yang, G. Sarma, D. H. Parker, J. J. ter Meulen, and L. Wiesenfeld, "State-to-state differential and relative integral cross sections for rotationally inelastic scattering of H_2O by hydrogen," Chem. Phys., preprint arXiv:1104.2715 (2011).
[49]V. Aquilanti, S. Cavalli, D. D. Fazio, A. Simoni, and T. V. Tscherbul, J. Chem. Phys. **123**, 054314 (2005).
[50]D. Sokolovshi, D. D. Fazio, S. Cavalli, and V. Aquilanti, Phys. Chem. Chem. Phys. **9**, 5664 (2007).
[51]F. Fernandez-Alonso, B. D. Bean, and R. N. Zare, J. Chem. Phys. **111**, 1035 (1999).
[52]S. E. Bradforth, D. W. Arnold, D. M. Neumark, and D. E. Manolopoulos, J. Chem. Phys. **99**, 6345 (1993).
[53]D. E. Manolopoulos, K. Stark, H. J. Werner, D. W. Arnold, S. E. Bradforth, and D. M. Neumark, Science **262**, 1852 (1993).
[54]F. J. Aoiz, V. J. Herrero, and V. S. Rábanos, J. Chem. Phys. **94**, 7991 (1991).
[55]S. Fleischer, Y. Khordorkovsky, Y. Prior, and I. S. Averbukh, New J. Phys. **11**, 105039 (2009).
[56]A. G. York, Opt. Express **17**, 13671 (2009).
[57]K. Kitano, H. Hasegawa, and Y. Ohshima, Phys. Rev. Lett. **103**, 223002 (2009).